Molecular beams with a tunable velocity

Cynthia E. Heiner,[a] Hendrick L. Bethlem[ab] and Gerard Meijer*[a]

Received 15th February 2006, Accepted 4th April 2006
First published as an Advance Article on the web 24th April 2006
DOI: 10.1039/b602260j

The merging of molecular beam methods with those of accelerator physics has yielded new tools to manipulate the motion of molecules. Over the last few years, decelerators, lenses, bunchers, traps, and storage rings for neutral molecules have been demonstrated. Molecular beams with a tunable velocity and with a tunable width of the velocity distribution can now be produced, and are expected to become a valuable tool in a variety of physical chemistry and chemical physics experiments. Here we present a compact molecular beam machine, capable of producing 3D spatially focused packets of state-selected accelerated or decelerated molecules.

1. Introduction

"Born in leaks, the original sin of vacuum technology, molecular beams are collimated wisps of molecules traversing the chambered void that is their theatre like companies of players framed by some proscenium arch. On stage for only milliseconds between their entrances and exits, they have captivated an ever growing audience by the variety and range of their repertoire." This is how John Fenn affectionately summarized the properties of molecular beams in 1987, in his foreword to volume 1 of the by now classic book *Atomic and Molecular Beam Methods*. His foreword continues with a brief overview of the history of molecular beams, mentioning the seminal contributions from the Stern and Rabi era, and remarks that "many if not most of the experiments that we may now regard as landmarks of the Chemical Era were anticipated, even tried, usually in vain, by investigators in those earlier times. Success when it came seems often to have been due almost as much to advances in supporting technology as to any of the many new ideas (..)".[1]

This article deals with the production of beams of polar molecules with a tunable velocity, beams that offer the possibility to extend the time that the "players are on stage" from milliseconds to seconds. Time-varying inhomogeneous electric fields are employed to gain full control over the motion of molecules, *e.g.* to accelerate or decelerate, and to transversally and/or longitudinally focus or cool a beam of polar molecules. The underlying operation principle is straightforward; it exploits the interaction between polar molecules and electric fields. This has been used extensively in the Stern and Rabi era to deflect and focus molecular beams, and is the basis of, for instance, the molecular beam electric resonance method and quantum-state selective (reactive) scattering experiments.[1] This same interaction can also be used to control the longitudinal velocity of molecular beams. When polar molecules in a so-called low-field seeking quantum state, *i.e.* with their space-fixed dipole moments anti-parallel to the electric field, enter an area of electric field their Stark energy increases. These molecules then experience a force opposing their motion and they slow down. If the electric field is switched off before the molecules have left the electric field region, they do not regain their lost kinetic energy. Thus, by letting the molecules pass through multiple pulsed electric fields they can be slowed down to arbitrarily low velocities.

The first experimental demonstration of the Stark deceleration of a beam of neutral polar molecules was given in 1999, when a beam of metastable CO molecules was slowed down from 225 to 98 m s^{-1} in an array of time-varying electric fields.[2] In accordance with the remark quoted above, experiments of this kind had been considered and tried before. Electric field deceleration of neutral molecules was first attempted by John King at MIT in 1958. He intended to produce a slow ammonia beam to obtain a MASER with an ultra-narrow linewidth.[3] However, in the physical chemistry and chemical physics community, the experimental efforts of Lennard Wharton, to demonstrate electric field acceleration of a molecular beam, are much better known. In the sixties, at the University of Chicago, he constructed an eleven meter long molecular beam machine for the acceleration of LiF molecules in high-field seeking states from 0.2 to 2.0 eV, aiming to use these high energy beams for reactive scattering studies.[4] Both of these experiments were unsuccessful, and were not continued after the PhD studies were finished.[5,6] Whereas interest in slow molecules as a MASER medium declined owing to the invention of the LASER, the molecular beam accelerator was made obsolete by gas dynamic acceleration of heavy species in seeded supersonic He and H_2 beams. It was actually John Fenn, in his measurements on the velocity distribution of these beams, who unambiguously demonstrated this approach for making high energy beams to be simpler and more versatile.[7]

Our efforts to manipulate the velocity of neutral polar molecules were originally inspired by both the exquisite control that was available over the motion of atoms and the simultaneous lack of a similar level of control for—arguably more interesting—molecules. We have been exploring the possibilities to manipulate molecular motion with electric fields, and have focused on the production of molecules with a sufficiently low kinetic energy that can be stored in a DC[8] or

[a] *Fritz-Haber-Institut der Max-Planck-Gesellschaft, Faradayweg 4-6, D-14195 Berlin, Germany. E-mail: meijer@fhi-berlin.mpg.de*
[b] *Laser Centre Vrije Universiteit, De Boelelaan 1081, 1081 HV Amsterdam, The Netherlands*

AC[9] electric trap, or in a storage ring.[10] The Stark decelerator in two distinct geometries demonstrated for CO molecules in both low-field seeking[2] and high-field seeking states,[11] has been the pivotal tool in these studies. These two kinds of decelerators are the realizations of the types of decelerators as envisioned by John King and Lennard Wharton, respectively. The ''advances in supporting technology'' that enabled us to experimentally realize these decelerators include: sufficient computing power to perform detailed design studies of the electrode geometries and 3D trajectory calculations, intense pulsed molecular beam sources, fast and reliable high voltage switches, and sensitive state-selective laser-based detection schemes.

The molecular beams that exit the Stark decelerator, with their tunable velocity and tunable velocity spread, are ideally suited for many applications. These decelerated beams can be used for high-resolution spectroscopic studies[12,13] and lifetime measurements,[14] taking advantage of the increased interaction times. We also anticipate that such beams are advantageous for molecular interferometry and molecular optics experiments.[15] These beams enable the study of (in)elastic collisions and reactive scattering as a function of collision energy, down to zero collision energy. Studies of this kind have thus far been performed by crossing molecular beams under a variable angle.[16–18] With decelerated beams, these experiments can be performed with an unprecedented energy resolution and in a fixed experimental geometry. As the deceleration process is quantum-state specific, the bunches of slow molecules that emerge from the decelerator are extremely pure, which can be of particular importance for inelastic collision studies. Moreover, the decelerated molecules are all naturally spatially oriented, allowing steric effects to be studied. For the latter studies, a weak guiding field is needed to maintain a well-defined orientation of the molecules on their way from the decelerator to the interaction zone.

The Stark decelerator for neutral polar molecules is the equivalent of a linear accelerator (LINAC) for charged particles. As outlined above, the quantum-state specific force that a polar molecule experiences in an electric field is exploited in a Stark decelerator. This force is rather weak, typically some eight to ten orders of magnitude weaker than the force that the parent ion experiences in an electric field. Nevertheless, this force suffices to achieve complete control over the motion of polar molecules, using techniques akin to those used for the control of charged particles. Most importantly, this means that transport of molecules through the decelerator can be performed by employing the principle of phase-stability. This principle, discovered independently by Veksler[19] and McMillan,[20] forms the basis for synchrotron-like charged particle accelerators, and can be viewed as the trapping of the particles in a travelling potential well formed by the accelerating fields. It thereby provides a method to keep a packet of molecules together throughout the decelerator and enables the transportation, acceleration or deceleration, and cooling of a sample of neutral molecules while maintaining the initial phase-space density,[21] *i.e.* the density of molecules in position and momentum space.

Phase-stability only ensures that a packet of molecules stays confined in longitudinal phase-space. It is also required to keep the molecules together in the transverse direction. For molecules in low-field seeking states, this can be achieved using static electric fields,[1] whereas dynamic focusing (alternate gradient focusing) needs to be applied for molecules in high-field seeking states.[22] Keeping the molecules transversally together was actually one of the main problems in the King and Wharton experiments. Ideally, the transverse focusing should be completely decoupled from the longitudinal motion. For this reason, spatially separated focusing and acceleration stages were incorporated into the original design of the Wharton machine. However, this made the machine unpractically long. We have instead opted for very compact designs of the decelerators, using the electric field sections simultaneously for transverse focusing and deceleration.[2,11] The coupling between the transverse and the longitudinal motion that is inherent to these decelerator geometries does not significantly deteriorate the overall performance, provided that the number of deceleration stages is limited.[23]

For most of the experiments with decelerated beams, it is highly desirable to focus the molecules exiting the decelerator into the interaction region. For molecules in low-field seeking states, transverse focusing can be achieved using electrostatic quadrupole or hexapole lenses.[1] Focusing in the forward direction can be achieved using a buncher,[24] an adaption of the device well-known in charged particle physics. Just as a hexapole provides a harmonic focusing force in the transverse direction, the electric field in the buncher provides such a focusing force along the beam direction, in the moving frame of the molecular beam. With this buncher, both focusing in real space (''spatial focusing'') and focusing in velocity space (''velocity focusing'' or ''longitudinal cooling'') can be performed.[24]

In this paper, we describe a compact deceleration beamline for neutral molecules, consisting of a pulsed source, a Stark-decelerator, and transverse and longitudinal focusing elements. Originally, our plans to perform deceleration of molecular beams using electric fields were met with some skepticism from specialists in the molecular beam community. In part, this probably stemmed from a reminder of the unsuccessful experiments from the past, particularly since those experiments were entrusted to an esteemed experimentalist like Lennard Wharton. Skepticism still remained even after the first successful demonstration of Stark deceleration; the strength of the merging of molecular beam methods with those of accelerator physics was not yet apparent. In particular, the beauty of phase-stability and its importance in a Stark decelerator were not always appreciated. Now that Stark deceleration, longitudinal focusing, and electric field trapping of neutral polar molecules have all been demonstrated, there still appears to be a lingering fear that these experiments are extremely large, complicated, and demanding. Here, we want to set this straight. The Stark deceleration molecular beam machine that is described here is compact, simple, and easy to implement. The whole beamline is only about 70 cm long, and is operated with only four high voltage switches and two high voltage power supplies, and yet allows for all the control over the molecules as outlined above. The different parts of the beamline are discussed individually, keeping the discussion of the source and of the Stark decelerator rather brief; for more

details the reader is referred to existing literature.[25,26] The description of the motion of the particles through the molecular beam machine is given in longitudinal position and momentum space; the use of such a phase-space description is common practice in accelerator physics and it is most insightful to discuss the dynamics in a molecular beamline in these terms. The operation principle of the buncher is explained in some more detail, and new measurements are presented on the longitudinal spatial and velocity focusing of decelerated beams of state-selected ammonia molecules. In addition, continuous tuning of the velocity of the ammonia beam, with subsequent 3D-spatial focusing into the interaction region, is demonstrated.

2. Manipulation of molecular motion

2.1. Cooling in a beam expansion

Molecular beams are indeed born out of a controlled leak, *i.e.* by letting a gas adiabatically expand from a container through a small hole into vacuum. In the free jet expansion region, the molecules undergo multiple collisions, resulting in translationally and rotationally cold molecules (around 1 K) in the beam. Although the vibrational cooling is generally less effective, the degree of vibrational excitation is normally low enough that it can be neglected.[1] For our experiments, not only the low temperature is important, but also a high density of molecules in the molecular beam is required; hence a pulsed beam is implemented. The amount of molecules per space interval (density) and velocity interval (temperature) is known as the phase-space density. We define the phase-space density as

$$D = n\Lambda^3, \tag{2.1}$$

where n is the number density and $\Lambda = (2\pi\hbar^2/mkT)^{1/2}$ is the thermal de Broglie wavelength. Eqn (2.1) is a measure of the de Broglie wavelength of the particles in terms of their separation, and is also referred to as the degeneracy parameter of a gas. As this parameter increases towards one, the particles gradually lose their individuality and quantum-degeneracy can occur.[27,28]

To evaluate the phase-space density of the beam during the expansion, the beam is assumed to be adiabatic, implying that

$$n = n_0 \left(\frac{T}{T_0}\right)^{1/(\gamma-1)}, \tag{2.2}$$

where T_0, n_0 and T, n are the temperatures and number densities of the gas in the container and in the beam, respectively, and γ is the Poisson coefficient.[1] The phase-space density of molecules in the beam, D, can then be expressed in terms of the initial phase-space density in the container, D_0, as

$$D = D_0 \left(\frac{T}{T_0}\right)^{\frac{5-3\gamma}{2(\gamma-1)}}. \tag{2.3}$$

For a monoatomic gas, $\gamma = \frac{5}{3}$, resulting in a phase-space density that remains constant during the expansion, *i.e.* $D = D_0$. Molecules have more degrees of freedom, therefore γ is closer to 1. In this case, the phase-space density decreases during the expansion. Note that in our definition, the phase-space density is integrated over all internal degrees of freedom. In the expansion, the internal temperature decreases and the population of the lowest level increases. The decrease in phase-space density is therefore merely a consequence of the entropy release associated with this internal cooling. The phase-space density of molecules in their ground state level will actually greatly increase. In our pulsed beam, produced by seeding 5% ammonia in xenon, the phase-space density of the $|J,MK\rangle = |1,-1\rangle$ component of the inversion doublet is on the order of 10^{-9}.[26]

2.2. Stark deceleration of polar molecules

The Stark decelerator uses the interaction of polar molecules in selected quantum-states with time-varying electric fields to manipulate their motion. Fig. 1 depicts the basic principle of the Stark decelerator. One deceleration stage is comprised of two parallel, cylindrical, metal rods. One of the rods is connected to a positive and its partner to a negative switchable high-voltage power supply; alternating rods are connected to each other. In this configuration, the Stark energy $W(z)$ of a molecule in a low-field seeking quantum state is periodic ($2L$) along the beam axis (z-axis). Suppose such a molecule is entering the field as illustrated in Fig. 1. This molecule gains Stark energy at the expense of kinetic energy. If nothing would be changed, this molecule would regain its kinetic energy upon exiting the field. However, switching off this field while the molecule is still in the electric field region, results in a permanent loss of kinetic energy. The kinetic energy that can be extracted in a single deceleration stage is typically 0.1–0.2 meV, whereas the initial kinetic energy of the molecules in the beam is at least 10–20 meV. Thus, in order to make a significant change to the molecule's velocity, the process needs to be repeated many times. This is accomplished by switching the fields such that $W(z)$ is repeatedly shifted over a distance L, keeping it synchronous with the movement of the molecules along the beam axis.[2]

The amount of energy that a molecule will lose depends on its position at the time that the fields are switched. Borrowing terms from particle accelerator physics, this position is

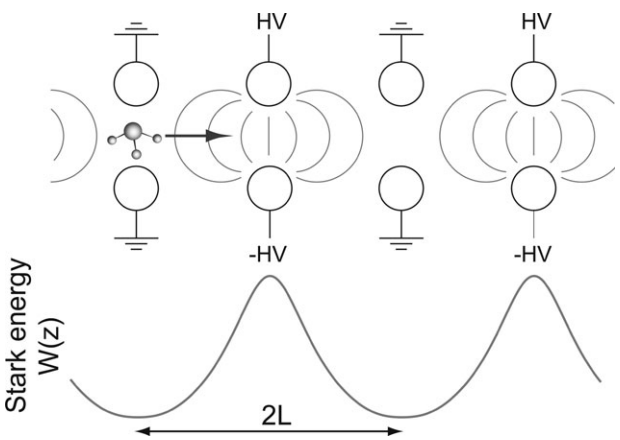

Fig. 1 Scheme of the Stark decelerator. The Stark energy of a ND_3 molecule in a low-field seeking quantum state is shown as a function of position z along the molecular beam axis. The Stark energy has a period of $2L$.

denoted as the "phase" or "phase-angle", $\phi = 2\pi(z/2L)$. Molecules that are in the maximum electric field just prior to the fields being switched off are assigned a phase-angle $\phi = 90^\circ$.[25] These molecules lose the maximum amount of energy possible per stage.

To describe the motion of an ensemble of molecules through the Stark decelerator, it is convenient to express their position and velocity relative to the position and velocity of a "synchronous molecule"—so called because the switching of the fields is synchronized to this particular molecule. The phase and velocity of the synchronous molecule are designated as ϕ_s and ν_s, respectively. The synchronous molecule always travels exactly a distance L in the time interval ΔT between switching the fields. Per definition it always has the same phase ϕ_s, and loses the same amount of kinetic energy per stage. To assure this, ΔT must be increased (decreased) as the synchronous molecule is decelerated (accelerated).

The relevance of the notion of a synchronous molecule is that other molecules, which are close to the synchronous molecule, feel a force towards the synchronous molecule. Let us consider a typical deceleration experiment with $\phi_s = 70^\circ$. A molecule slightly ahead of the synchronous molecule, but with the same velocity, loses more energy per stage than the synchronous molecule. Hence, it is slowed down with respect to the synchronous molecule, and consequently its phase becomes smaller. This process repeats itself until the molecule's phase has become smaller than ϕ_s, at which point it lags behind the synchronous molecule. Now the situation is reversed and this molecule loses less energy, *i.e.* it speeds up, with respect to the synchronous molecule, *etc.* This example shows that molecules with phase-space coordinates slightly different from (ϕ_s, v_s) oscillate both in phase and velocity around the synchronous molecule; the molecules are trapped in a travelling potential well moving along with the synchronous molecule. This is known as phase-stability. Note that in phase-space, the non-synchronous molecules rotate around the position of the synchronous molecule.

The range of positions and velocities that are accepted by the decelerator are determined by the phase-angle of the synchronous molecule, which is set to $0 < \phi_s \leq 90^\circ$ for deceleration experiments. The larger the phase-angle, the more kinetic energy is extracted per stage. However, the number of molecules that are accepted is largest for small phase-angles. As both a large deceleration and a large acceptance are needed, a compromise must be found, typically ϕ_s is chosen between 50 and 70°.

Fig. 2 shows the calculated phase-space distribution of an ensemble of ammonia molecules as they pass through the decelerator. For eight different times, the longitudinal velocities of the molecules are given as a function of their position along the beam axis. In this simulation, the fields are switched such as to decelerate from 272 to 92 m s^{-1} using a synchronous phase of $\phi_s = 70^\circ$. The forward tilting of the phase-space distribution with increasing time reflects the (almost) free flight of the molecules that are not accepted by the decelerator. A packet of molecules is seen to stay together as a "bunch" while it is being decelerated. In fact, a few decelerated bunches, trailing each other by a distance of 11 mm, are observed. This results from the position spread of the beam being about 25

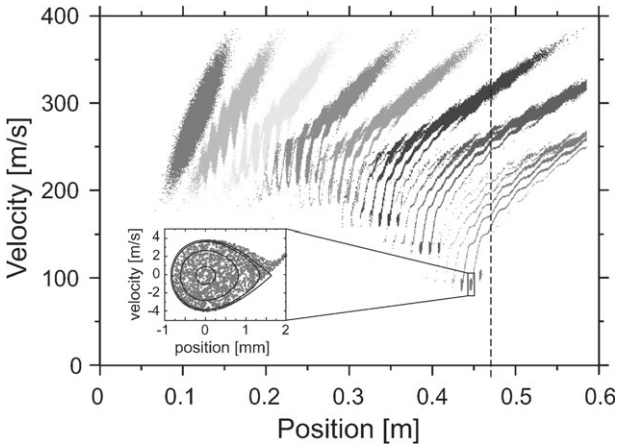

Fig. 2 Numerical simulations of the phase-space distribution of an ensemble of ND_3 molecules passing through the decelerator for eight different times. In the inset, the phase-space distribution of a decelerated packet is shown in the moving frame of the synchronous molecule. The dashed vertical line indicates the position at which the TOF measurements shown in Fig. 6 are taken.

mm at the entrance of the decelerator, which is more than twice the period $2L = 11$ mm. Therefore, more than one travelling well ("bucket") will be filled. The inset shows the longitudinal phase-space distribution of a decelerated bunch relative to the position of the synchronous molecule, *i.e.* in the moving frame (z,v) of the synchronous molecule. The decelerated packet has a position spread of 2 mm and a velocity spread of 8 m s^{-1}. The solid curves in the inset result from a simple model for phase-stability.[21] Note that for a given decelerator geometry, the position and velocity spread are independent of the initial and final velocity, but are rather solely determined by the phase-angle. The phase-space density of the packet stays constant throughout the deceleration process, as dictated by the Liouville theorem.

Thus far, we have only discussed the longitudinal dynamics of the molecules through the decelerator. To establish transverse stability, successive pairs of electrodes are orientated at 90° angles relative to each other.[2] As the electric field is highest near the electrodes, molecules in low-field seeking states are then focused towards the molecular beam axis in both transverse directions while passing through the decelerator. When operated at a phase angle of $\phi_s = 70^\circ$, our decelerator accepts molecules with transverse position and velocity spreads of 2 mm and 5 m s^{-1}, respectively.[25]

2.3. Bunching and focusing

As described above, the Stark decelerator can be used to produce a packet of molecules with a well-defined distribution in phase-space. Upon leaving the decelerator, this confined distribution spreads out, both longitudinally and transversally. During free-flight, the longitudinal phase-space distribution of the packet elongates. The faster molecules pull ahead of the synchronous molecule while the slower ones lag behind; thus, the free-flight establishes a linear relation between the position of the molecule and its velocity. After free-flight over a distance L_1, a buncher is used to longitudinally focus the

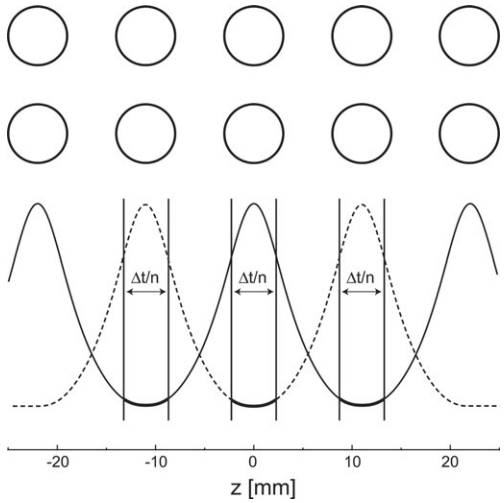

Fig. 3 Schematic drawing of the buncher, together with the Stark energy of a molecule in a low-field seeking state as a function of position z along the molecular beam axis.

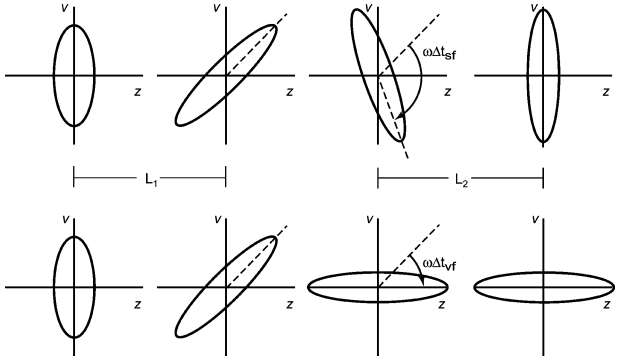

Fig. 4 Sketches of the longitudinal phase-space distribution at four different times, namely when the synchronous molecule is at the exit of the decelerator, the entrance of the buncher, the exit of the buncher, and the interaction region. The upper and lower series illustrate spatial and velocity focusing, respectively. For spatial focusing the packet is rotated in phase-space over 180°, in going from the exit of the decelerator to the interaction region; for velocity focusing, this rotation is over 90°.

molecules into the interaction region, which is located a further free-flight distance L_2 away. Hexapoles are used before and after the buncher to transversally focus the molecules into the buncher and into the interaction region, respectively.

A schematic drawing of the buncher is shown in Fig. 3. The buncher consists of five pairs of electrodes, each comprised of two parallel, cylindrical, metal rods. The rods are connected to either a positive or negative switchable high-voltage power supply. Alternating rods are separated by a center-to-center distance of 22 mm and are connected to each other. In this figure, the Stark energy of a molecule in a low-field seeking state along the molecular beam axis is given for the case that either the odd (solid curve) or even (dotted curve) pairs of electrodes are switched to high voltage, while the others are grounded. The electric field in the buncher is turned on for a total time Δt. The field in the buncher is switched on when the synchronous molecule arrives at the position indicated with the left-most vertical line in Fig. 3; the field is switched off again when it arrives at the position indicated by the next vertical line. During this time-interval (marked by $\Delta t/n$ in the figure), the synchronous molecule is equally accelerated and decelerated, as it spends the same amount of time on the downward and upward slopes of the Stark potential, respectively. Molecules ahead of the synchronous one, *i.e.* molecules that were originally faster, spend more time on the upward slope than on the downward slope of the potential, and thus are decelerated with respect to the synchronous molecule. Likewise, molecules that are behind the synchronous molecule are accelerated with respect to the synchronous molecule. This process is repeated n times, where n has a maximum value of three for the present buncher.

The longitudinal phase-space distribution is sketched in Fig. 4 at four different times, for two different time-intervals that the buncher is on. The distributions are shown in the moving frame of the synchronous molecule, *i.e.* the synchronous molecule is always located at the origin. The phase-space distributions are plotted when the synchronous molecule is at the exit of the decelerator, the entrance and exit of the buncher, and the interaction region. Clearly seen here is the elongation and tilting of the phase-space distribution during free-flight over the distance L_1. During the time Δt that the buncher is on, the longitudinal phase-space distribution is uniformly rotated, with an angular frequency ω, in the (z,v)-plane. In the upper part of Fig. 4, Δt is chosen such that a spatial focus is formed in the interaction region. When the buncher is on for a shorter time, the distribution is rotated over a smaller angle $\omega\Delta t$. This is sketched in the lower part of Fig. 4, where the longitudinal velocity spread is minimized—this "velocity cooling" is equivalent to creating a spatial focus at infinity. Keeping in analogy with charged particle physics's terms, the spatial and velocity focusing are referred to as "re-bunching" and "bunch rotation," respectively.[24]

The time-interval that the buncher needs to be turned on can be analytically evaluated using a simple matrix method. With this method, the final position of a molecule in longitudinal phase-space (z',v') can be determined as follows

$$\begin{pmatrix} z' \\ v'/\omega \end{pmatrix} = \boldsymbol{M} \begin{pmatrix} z \\ v/\omega \end{pmatrix}. \qquad (2.4)$$

where $\boldsymbol{M}$ is the transfer matrix, and (z,v) is the original position of the molecule in phase-space. Note that these coordinates are all in the moving frame of the synchronous molecule. Dividing the velocity by the angular frequency, ω, has the advantage that the elements of the transfer matrix become dimensionless. The transfer matrix that describes the molecular motion during free flight over L_1, within the buncher, and during free flight over L_2 can be written as the product

$$\boldsymbol{M} = M_{O1} M_F M_{O2} \qquad (2.5)$$

with

$$\begin{aligned} M_{O1} &= \begin{pmatrix} 1 & \omega\frac{L_1}{v_s} \\ 0 & 1 \end{pmatrix} && \text{free flight} \\ M_F &= \begin{pmatrix} \cos\omega\Delta t & \sin\omega\Delta t \\ -\sin\omega\Delta t & \cos\omega\Delta t \end{pmatrix} && \text{buncher} \\ M_{O2} &= \begin{pmatrix} 1 & \omega\frac{L_2}{v_s} \\ 0 & 1 \end{pmatrix} && \text{free flight} \end{aligned} \qquad (2.6)$$

We can use the approximation that $\omega\Delta t \ll 1$, *i.e.* $\cos\omega\Delta t \approx 1$ and $\sin\omega\Delta t \approx \omega\Delta t$, and that $\Delta t \ll (L_1+L_2)v_s$. This enables us to calculate the time-interval Δt, needed for a molecule to arrive in the interaction region simultaneously with the synchronous molecule. This is done by setting $z' = 0$ in eqn (2.4) and solving for Δt, as a function of the initial phase-space position (z,v). The result can be written as:

$$\Delta t|_{z'=0}(z,v) = \frac{v_s(zv_s + v(L_1+L_2))}{\omega^2 L_2(zv_s + vL_1) - vv_s^2}. \quad (2.7)$$

Likewise, we can calculate the time-interval Δt, such that a molecule has the same velocity as the synchronous molecule at the time that the latter arrives in the interaction region. For this, $v' = 0$ in eqn (2.4), leading to:

$$\Delta t|_{v'=0}(z,v) = \frac{vv_s}{\omega^2(zv_s + vL_1)}. \quad (2.8)$$

Eqn (2.7) and eqn (2.8) describe a distribution of time-intervals Δt. At the peak of the $\Delta t|_{z'=0}(z,v)$ distribution, there is a maximum number of molecules that arrive in the interaction region simultaneously with the synchronous molecule, *i.e.* a spatial focus is achieved. Similarly, at the peak of the $\Delta t|_{v'=0}(z,v)$ distribution, there is a maximum number of molecules that have obtained the same velocity as the synchronous one, *i.e.* a velocity-focus is achieved. As the original phase-space distribution (z,v) is centered around (0, 0), it follows that the spatial focus is obtained at

$$\Delta t_{sf} = \frac{v_s(L_1+L_2)}{\omega^2 L_1 L_2 - v_s^2}. \quad (2.9)$$

Likewise, from eqn (2.8), the velocity focus is obtained at

$$\Delta t_{vf} = \frac{v_s}{\omega^2 L_1}. \quad (2.10)$$

As expected, eqn (2.9) reduces to eqn (2.10) when L_2 goes to infinity. An interesting observation, when comparing the distributions given by eqn (2.7) and eqn (2.8), is that the relative width of the $\Delta t|_{z'=0}$ distribution is narrower than that of the $\Delta t|_{v'=0}$ distribution.

Briefly, we address the transverse focusing of the hexapoles. Our hexapoles consist of six cylindrical rods with radius r placed equidistantly around a circle with radius $2r$. The rods are alternatingly at ground potential and at high voltage, creating a cylindrically symmetric electric field that is zero at the molecular beam axis, and increases further outwards. Molecules in low-field seeking states with a linear Stark effect experience a harmonic restoring force towards the molecular beam axis.[1] Rather than the common practice of applying a constant voltage to the hexapole rods, we apply the electric field for a short time-interval. This enables us to effectively vary the focusing strength and position of the hexapole lens. The motion of the molecules through the hexapole in the transverse direction can be evaluated using the matrix method, in the same manner as above.

3. Experimental setup

The compact molecular beam machine used for the present experiments is shown schematically in Fig. 5, and is pictured below it. The apparatus consists of two differentially pumped

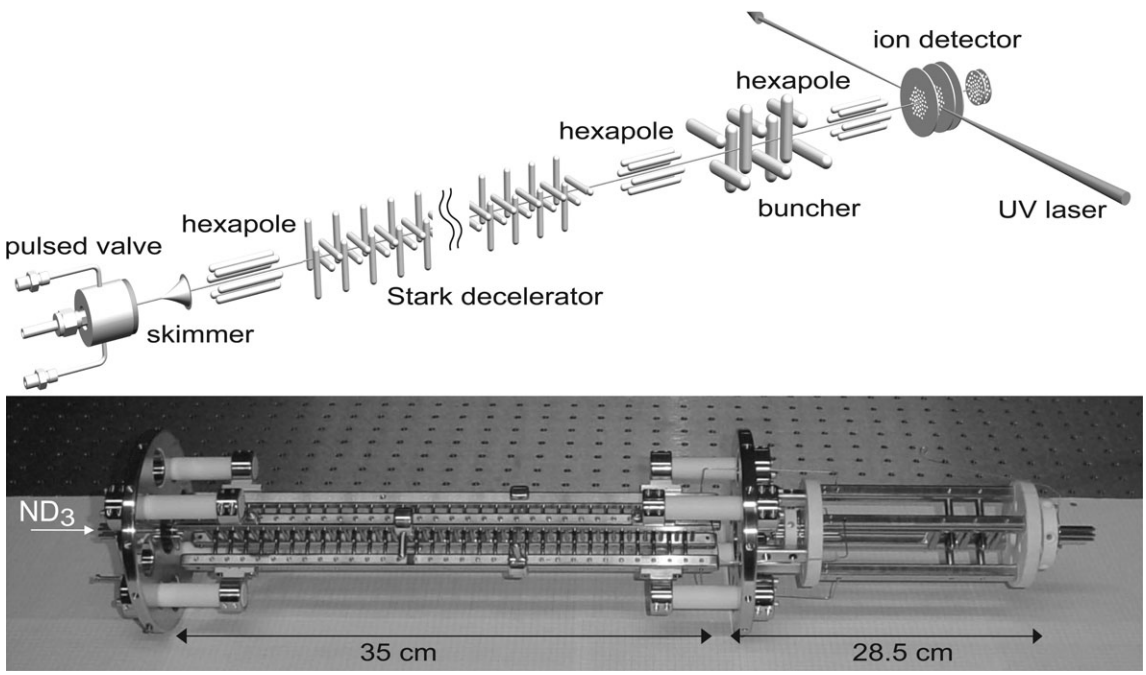

Fig. 5 Scheme of the molecular beam machine. ND_3 molecules seeded in Xe expand through a nozzle at a 10 Hz rate. After passing through a skimmer, molecules in the low-field seeking $|J,KM\rangle = |1,-1\rangle$ level are focused with a hexapole into the Stark decelerator. The decelerated molecules pass through a hexapole–buncher–hexapole combination prior to entering the detection region. There, the density of the ammonia molecules is state-selectively detected using a UV-laser ionization scheme (2 + 1 REMPI). Below, a photo is shown of the main components: (from left to right) hexapole, decelerator, hexapole, buncher, hexapole.

vacuum chambers separated by a skimmer with a 1 mm diameter opening. The source and decelerator chambers are both pumped by 500 l s^{-1} turbo pumps. A gas mixture comprising about 5% ND_3 in xenon at a backing pressure of 2 atm is expanded into vacuum using a solenoid valve pulsed at 10 Hz. The solenoid valve (General Valve Series 9) is modified such that it can be operated down to liquid nitrogen temperatures. In these experiments, the valve is cooled to 200 K, and opens for a duration of 100 μs. Under operation conditions, the pressure in the source and deceleration chamber is typically 8×10^{-6} and 2×10^{-8} mbar, respectively. In the molecular beam, only the lowest rotational levels in the electronic and vibrational ground state are occupied. In our beam, *ca.* 60% of all ND_3 molecules reside in the ground state of para-ammonia, of these one-fourth are found in the low-field seeking $|J,KM\rangle = |1,-1\rangle$ level.[25]

After passing through the skimmer, the beam is focused with a pulsed hexapole into the Stark decelerator. The Stark decelerator consists of 63 pairs of highly polished, stainless steel electrodes, and has a total length of 35 cm. The cylindrical electrodes have a diameter of 3 mm and are separated by 5 mm (center-to-center), leaving a 2 mm gap for the molecular beam to pass through. Successive electrode pairs are separated by a center-to-center distance of $L = 5.5$ mm, and are alternatingly orientated horizontally and vertically. The electrodes are suspended by four metal bars, which are connected to two positive and two negative high voltage switches. In these experiments, a voltage difference of 20 kV is applied across an electrode pair, creating a maximum electric field of 90 kV cm^{-1} on the molecular beam axis.

After exiting the Stark decelerator, the molecules pass through a second pulsed hexapole, and are focused into the buncher, a distance of $L_1 = 192$ mm away. The buncher consists of five electrode pairs, with successive pairs separated by a center-to-center distance of 11 mm; the geometry of the buncher is identical to that of our decelerator, with the dimensions scaled up by a factor of two. Behind the buncher, a third pulsed hexapole is mounted. All three hexapoles are comprised of six, cylindrical, stainless steel rods with a radius $r = 3$ mm and a length of 50 mm. In these experiments, the second and the third hexapoles are only switched on for up to 25 μs, corresponding to an effective length of only a few millimeters. The effective position of these electrostatic lenses can be varied over almost the full length of the hexapole. It is advantageous to use high fields in the hexapole for short times, instead of using low fields for long times, as this reduces the unwanted effects of non-linearities associated with the inversion splitting in ammonia.

Finally, the molecules travel into the detection region at a distance $L_2 = 170$ mm behind the buncher, implying a total length of the beamline of about 70 cm. For some of the measurements, we have increased L_2 to 3400 mm (this is not a typo!), by coupling the molecules into a storage ring.[10] The molecules in the $|J,K\rangle = |1,1\rangle$ upper component of the inversion doublet are detected here *via* a (2 + 1) resonance enhanced multi photon ionization (REMPI) scheme. The laser light, with a typical energy of 16 mJ around 317 nm in a 5 ns duration pulse, is focused in the interaction region using a lens with a 75 cm focal length. Parent ions are mass-selectively detected using a Wiley–McLaren-type linear time-of-flight mass spectrometer. The ion signal is proportional to the density of the ammonia molecules in the interaction region.

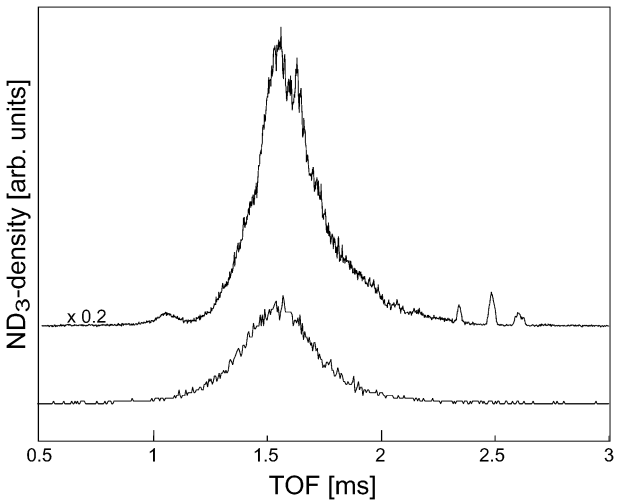

Fig. 6 Density of ND_3 molecules recorded 25 mm behind the decelerator as a function of time after release of the gas pulse. The lower and upper curves show the TOF profiles of the original and decelerated (272 to 92 m s^{-1}) beams, respectively. At least three bunches of slow molecules are seen to arrive in the detection region about 1 ms later than the original beam. Note that the signal of the decelerated beam is increased by more than an order of magnitude due to transverse focusing when the decelerator is switched on.

The Stark decelerator, buncher, and hexapoles are all suspended and isolated using ceramics. They are mounted and aligned as one unit, as shown in the photo in Fig. 5. The decelerator, the buncher, and the hexapoles are all electrically connected. The switching of the entire unit is then accomplished with only four fast, high voltage switches (Behlke Electronic GmbH, HTS-151-03-GSM), and using two high voltage power supplies (FUG, HCN 700-12500). A residual bias voltage of +150 V is applied to the positive electrodes to prevent Majorana transitions to the $|J,KM\rangle = |1,0\rangle$ level, which is not a low-field seeking state. The switches are triggered by a programmable delay generator running at a clock frequency of 100 MHz. The sequence of timings, during which fields are switched, is generated using a computer program that calculates the trajectory of the synchronous molecule through the beam machine. Typical time sequences last for less than 10 ms, and a new time sequence can be loaded at a 10 Hz rate.

4. Experimental results

To demonstrate the performance of the Stark decelerator, we first present measurements taken directly behind the decelerator; these same measurements have been shown and discussed earlier.[25] In Fig. 6, the density of the ND_3 molecules 25 mm behind the decelerator is shown as a function of time after release of the gas pulse. The lower curve shows the time-of-flight (TOF) profile of the original, undecelerated beam. The mean velocity of the ammonia molecules in the beam is 285 m s^{-1}. The velocity spread of the beam (FWHM) is *ca.*

20%, corresponding to a translational temperature of 1.6 K. The upper curve shows the TOF profile when the Stark decelerator is used to slow down the molecules from 272 to 92 m s^{-1} using a phase-angle of 70°. Three bunches of slow molecules are seen to arrive in the detection region about 1 ms after the original beam. The transverse focusing in the decelerator leads to an increase of signal by more than an order of magnitude when the voltages are turned on. In fact, even the decelerated signal is larger than the peak intensity of the original beam. Note that the parameters used to calculate the phase-space distributions presented in Fig. 2 are the same as in this measurement.

Of the three decelerated bunches in Fig. 6, the central (main) bunch contains molecules that had their initial position and velocity centered around those of the synchronous molecule, and passed through all the deceleration stages. The earlier bunch contains molecules, with the same initial velocity of 272 m s^{-1}, that were located already inside the decelerator when it was first switched on; throughout the decelerator, they travelled 11 mm ahead. They missed the last two stages of deceleration, and therefore exit with a slightly higher velocity of 102 m s^{-1}, which actually can be nicely seen in Fig. 2. The later bunch contains molecules which had a lower initial velocity of 268 m s^{-1}, exactly one period's worth less of energy, and entered the decelerator one period later. These molecules trail the main bunch by exactly 11 mm throughout the decelerator, and are still in the decelerator when the electric fields are turned off. These molecules therefore have the same final velocity of 92 m s^{-1}.

To demonstrate the performance of the buncher, measurements are taken at two different distances L_2 behind the buncher. For these experiments, ammonia molecules are decelerated from an initial velocity of 266 m s^{-1} to a velocity of 85 m s^{-1} at the exit of the decelerator. The longitudinal phase-space distribution (z,v) of the decelerated package is the one presented in the inset of Fig. 2, as the phase-angle of the Stark decelerator is set at 70°. In the center panel of Fig. 7, the density of ND_3 molecules in the interaction region is shown as a function of the time that the buncher is turned on. The angular frequency, ω, experienced by the ND_3 molecules in the buncher is 2450 rad s^{-1}. The buncher is operated here with two stages ($n = 2$), and the total Δt is shown on the horizontal axis. The molecules are detected at the moment that the synchronous molecule is at the center of interaction region. We will refer to the measurements taken at a distance $L_2 = 170$ mm behind the buncher as spatial focusing, whereas the measurements taken at $L_2 = 3400$ mm (a spatial focus far away) will be referred to as velocity focusing. Both of these measurements are best denoted as longitudinal focusing curves, in analogy with the well-known hexapole focusing curves.[1] The gray curves are the analytically calculated longitudinal focusing curves, that directly follow from eqn (2.7), using the experimental values for v_s, L_1, L_2, ω, and the initial-phase space distribution as given in Fig. 2. For the Δt values marked with solid circles on either one of the experimental longitudinal focusing curves, time-of-flight measurements are performed. These measurements are displayed in the right and left panels of Fig. 7, and show the arrival time distribution of the molecules in the interaction region for $L_2 = 170$ mm and $L_2 = 3400$ mm, respectively. The horizonal axis gives the time relative to the release of the gas pulse. The different TOF

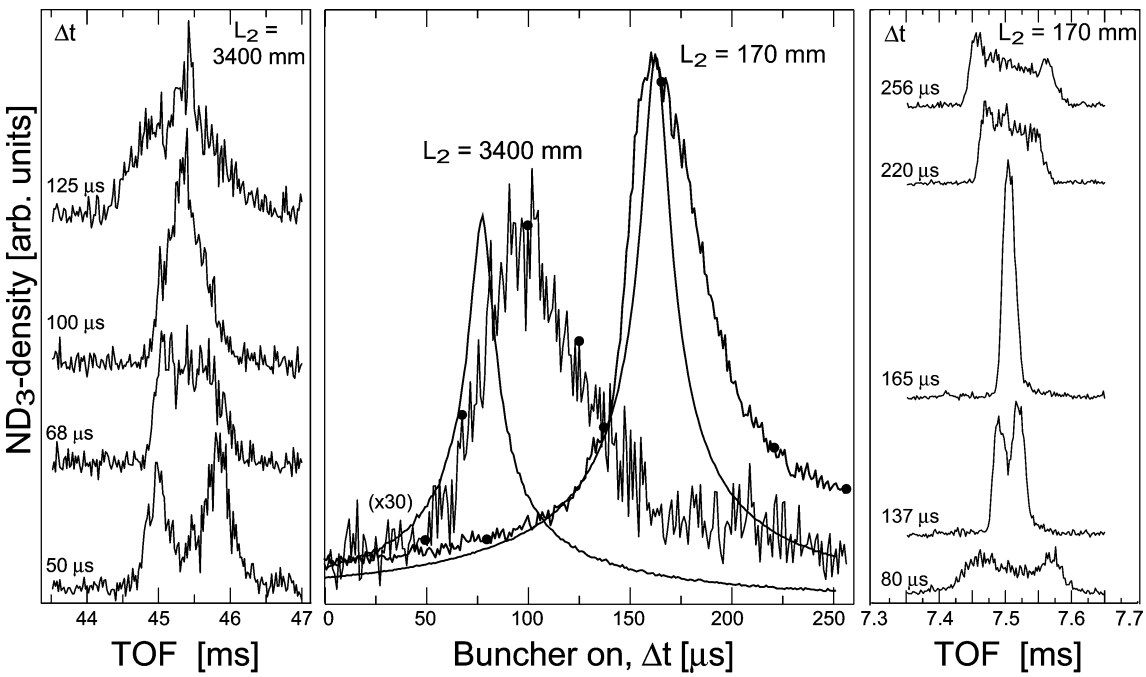

Fig. 7 In the center panel, measurements are shown of the density of ND_3 molecules, at two different positions L_2 behind the buncher, as a function of the total time Δt that the buncher is on, together with analytically calculated distributions. These longitudinal focusing curves are measured when the synchronous molecule is in the interaction region. The solid circles on these curves mark the bunching times used to obtain the TOF profiles, shown in the left and right panels (at $t = 0$ the gas pulse is released). The measured TOF profiles are given an offset for clarity, and within each series the vertical scale is the same.

profiles are given an offset for clarity, and within each series the vertical scale is the same. The integrated intensity of either series remains almost constant (to within 10%).

The peak of the spatial focusing curve (L_2 = 170 mm) is found at Δt = 162 μs, in agreement with the value of Δt_{sf} = 163 μs found from eqn (2.9). The calculated spatial focusing curve is considerably narrower than the measured one. This results from the neglect of the limited acceptance of the buncher in the calculation; the model does not take into account that the length of the (harmonic part of the) focusing potential in the buncher is finite. In order to get sufficiently far away from the buncher, to record the velocity focusing curve (L_2 = 3400 mm), the molecules are injected into a 80 cm circumference storage ring, and are detected after four round trips. The peak of the velocity focusing curve is found at Δt = 100 μs, at a shorter buncher time than that of the spatial focusing curve, as expected. The calculated velocity focusing curve does not agree well with the measurements. For velocity focusing, the non-linearities of the buncher potential are more critical. Moreover, the transverse (betatron) oscillations of the molecules in the storage ring couple to the forward (tangential) motion, by conservation of angular momentum.[29] Therefore, the longitudinal velocity distribution can be expected to be modified.

The series of time-of-flight profiles, displayed on either side in Fig. 7, nicely show the transition from an under-focused distribution, *via* a focus, to an over-focused distribution. In the focus at L_2 = 170 mm, the length of the packet, as deduced from the width of the TOF profile, is about 2 mm. In this case an (almost) 1 : 1 image of the packet at the exit of the decelerator is made in the interaction region, about 36 cm further downstream. In the focus at L_2 = 3400 mm, the length of the packet is about an order of magnitude larger. This implies that the width of the velocity distribution is reduced by an order of magnitude relative to the distribution at the exit of the decelerator, hence the longitudinal temperature is decreased by two orders of magnitude. The structures observed in the TOF profiles can be fully explained by including the non-linearities in the buncher, as discussed elsewhere.[24,29]

In Fig. 8, the density of ND_3 molecules is shown in the interaction region, 36 cm behind the decelerator, as a function of velocity. The forward velocity of the ammonia beam in the interaction region is continuously scanned in steps of 1 m s^{-1} over the 55–130 m s^{-1} range. This tuning is accomplished here, by selecting a different initial velocity in the 257–283 m s^{-1} range, *i.e.*, by changing the time-delay between the triggering of the pulsed valve and the switching on of the Stark decelerator. The Stark decelerator is operated at the same phase-angle of 70° throughout these measurements. For each velocity, the settings of the hexapoles and the buncher (n = 3) are adjusted such as to create a 3D-spatial focus in the interaction region. Note that in this way, the length of the decelerated beam in the interaction region is always the same (about 2 mm). The data points shown in Fig. 8 are averaged over 64 shots. For each new velocity, a new time-sequence, with the pre-calculated optimum timings for the decelerator, hexapoles, and buncher, is loaded. The total time it takes to perform the velocity scan, as shown in the figure, is therefore less than 10 min. The reduction in signal that is observed for lower final velocities, results in part from the reduced number of molecules at the initial velocity in the beam. In addition, the finite acceptance of the hexapoles and buncher limits the signal intensity for low velocities; the transverse and longitudinal spreading out of the beam are inversely proportional to the forward velocity and, for low velocities, only part of the beam can be refocused.

To give yet another example of the possibilities of this compact beamline, we demonstrate in Fig. 9 the production and simultaneous 3D-spatial focusing of two packets of ammonia molecules, each with a slightly different forward velocity. The individual packets arrive in the interaction region about 125 μs apart. The packets originate from the same gas pulse, and are created by purposely loading two "buckets" of the decelerator simultaneously, as explained in the discussion of Fig. 2 and Fig. 6. The first of these two "buckets" is loaded with molecules with an initial velocity of 266 m s^{-1}, which are decelerated to a final velocity of 85 m s^{-1}. The trailing "bucket" is filled with molecules that entered the decelerator

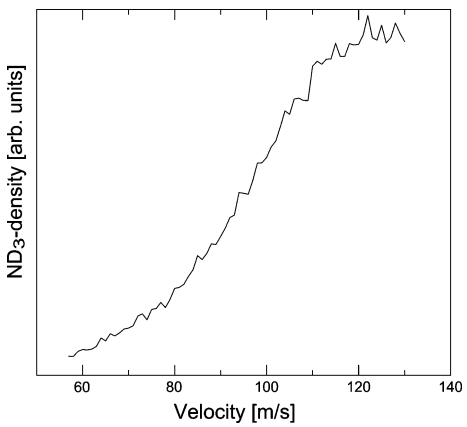

Fig. 8 The density of ND_3 molecules 36 cm behind the decelerator as a function of velocity. For each velocity, the molecules are 3D-spatially focused into the interaction region.

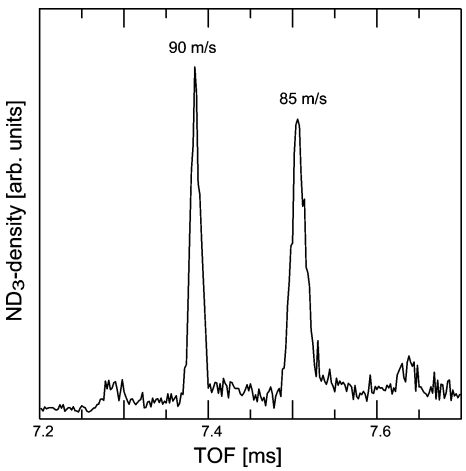

Fig. 9 Density of ND_3 molecules 36 cm behind the decelerator as a function of time after release of the gas pulse. Two 3D-spatially focused packets of molecules with forward velocities as indicated are observed. The length of each packet is about 2 mm, the separation between the packets is about 11 mm.

one period later, with a reduced initial velocity of 262 m s^{-1}. These molecules are also decelerated to 85 m s^{-1}, but already reach this velocity when they are still one period away from the end of the decelerator. As the leading packet is already at the exit of the decelerator at this time, we can use the electric fields in the last period of the decelerator to selectively change the velocity of the trailing packet. In this experiment, we have applied the electric fields such that the trailing packet is accelerated to a final velocity of 90 m s^{-1}. At this velocity, this packet catches up with the leading packet at the center of the buncher. The two decelerated packets are then longitudinally focused simultaneously. Similarly, the hexapoles on either side of the buncher simultaneously focus both packets transversally. In the interaction region, the faster molecules, *i.e.* the ones that exited the decelerator last, arrive first. As the buncher is positioned almost half-way between the decelerator and the detection point, the 3D-spatially focused packets of molecules are again separated by about 11 mm in the interaction region.

5. Conclusions and outlook

In this paper, we present a compact machine for the production of 3D-spatially focused beams of polar molecules with a tunable velocity, and with a tailored velocity distribution. The operation principles of the main components of this beam machine are outlined, and the performance of the decelerator beamline is demonstrated, using ammonia as a prototypical polar molecule. In the experiments presented here, the velocity of the beam of state-selected ammonia molecules has been varied in the 285–55 m s^{-1} range. By using different seed gases and/or by setting the pulsed valve at different temperatures, the full 0–2000 m s^{-1} can be covered with this beam machine. The laboratory velocity of a Stark decelerated beam is known to a very high precision, as it is only determined by the mechanical precision of the decelerator and by the accuracy of the timings of the high voltage switches; the experimental accuracy of the velocity of the synchronous molecule is better than 10^{-3}. The width of the velocity distribution of the decelerated beam is determined by the phase-angle of the decelerator and whether or not additional velocity focusing is applied, and is typically between 1–10 m s^{-1}. Together, this implies that this beam machine can be used for state-to-state scattering experiments with ammonia, for instance, covering the 0–400 meV range with an energy resolution that scales linearly with velocity, but that even at 400 meV is only about 1 meV.

Up till now, most of our deceleration and trapping experiments have used ammonia molecules. However, there are many other small polar molecules for which these methods are applicable. A list of possible candidate molecules, together with their relevant properties, is given in Table 1 of ref. 25. To date, Stark deceleration has been demonstrated for metastable CO (a $^3\Pi$),[2] different isotopomers of ammonia,[8,25] OH,[30,31] formaldehyde,[32] metastable NH (a $^1\Delta$),[33] and SO_2.[34] Deceleration and focusing of atoms and molecules in Rydberg states have also been demonstrated.[35,36] Additionally, Stark deceleration has been shown for the deceleration[11] and trapping[9] of molecules in their high field seeking states and has been applied to decelerate heavy polar molecules like YbF[37] and CaF,[38] as well as more complex, polyatomic molecules such as benzonitrile (our lab).

Molecular beams with a tunable velocity, as presented here, are a fascinating new tool to have around in the laboratory. For us, it has been an exciting and rewarding experience, to understand and choreograph the intricate phase-space dance of the "players on stage". This research originated in the Department of Molecular and Laser Physics at the University of Nijmegen, The Netherlands, which has a long history of molecular beam research.[1] *Via* a brief stay at the FOM—Institute for Plasmaphysics in Nieuwegein, The Netherlands, the experiments have now found their new home at the Fritz Haber Institute in Berlin, Germany, interestingly enough in the monumental hall that Fritz Haber used when working on the synthesis of our favorite molecule. Thus far, we have naturally concentrated on the development and testing of decelerators and focusing and trapping elements. By now, this machinery has sufficiently matured to the point where it can, and should, be used for a wide variety of molecular physics studies. We hope that this article helps to convince our colleagues of this as well.

Acknowledgements

We gratefully acknowledge the contributions of many colleagues to the experiments described in this paper, in particular, David Carty, Floris Crompvoets, Jacqueline van Veldhoven, Jochen Küpper, André van Roij, Henrik Haak, and Georg Heyne. H. L. B. acknowledges financial support from the Netherlands Organisation for Scientific Research (NWO) *via* a VENI-grant.

References

1 *Atomic and molecular beam methods*, ed. G. Scoles, vol. 1 & vol. 2, Oxford University Press, 1988 & 1992.
2 H. L. Bethlem, G. Berden and G. Meijer, *Phys. Rev. Lett.*, 1999, **83**, 1558.
3 J. G. King and J. R. Zacharias, *Quarterly Progress Report*, Research Laboratory of Electronics, Massachusetts Institute of Technology, 15 January 1958, 48.
4 R. Wolfgang, *Sci. Am.*, 1968, **219**, 44.
5 R. Golub, *On decelerating molecules*, PhD thesis, Massachusetts Institute of Technology, Cambridge, USA, 1967.
6 E. E. A. Bromberg, *Acceleration and alternate-gradient focusing of neutral polar diatomic molecules*, PhD thesis, University of Chicago, USA, 1972.
7 N. Abuaf, J. B. Anderson, R. P. Andres, J. B. Fenn and D. G. H. Marsden, *Science*, 1967, **155**, 997.
8 H. L. Bethlem, G. Berden, F. M. H. Crompvoets, R. T. Jongma, A. J. A. van Roij and G. Meijer, *Nature*, 2000, **406**, 491.
9 J. van Veldhoven, H. L. Bethlem and G. Meijer, *Phys. Rev. Lett.*, 2005, **94**, 083001.
10 F. M. H. Crompvoets, H. L. Bethlem, R. T. Jongma and G. Meijer, *Nature*, 2001, **411**, 174.
11 H. L. Bethlem, A. J. A. van Roij, R. T. Jongma and G. Meijer, *Phys. Rev. Lett.*, 2002, **88**, 133003.
12 J. van Veldhoven, J. Küpper, H. L. Bethlem, A. J. A. van Roij and G. Meijer, *Eur. Phys. J. D*, 2004, **31**, 337.
13 E. R. Hudson, H. J. Lewandowski, B. C. Sawyer and J. Ye, *Phys. Rev. Lett.*, **96**, 143004.
14 S. Y. T. van de Meerakker, N. Vanhaecke, M. P. J. van der Loo, G. C. Groenenboom and G. Meijer, *Phys. Rev. Lett.*, 2005, **95**, 013003.
15 M. Arndt, O. Nairz, J. Vos-Andreae, C. Keller, G. van der Zouw and A. Zeilinger, *Nature*, 1999, **401**, 680.

16 G. H. Hall, K. Liu, M. J. McAuliffe, C. F. Giese and W. R. Gentry, *J. Chem. Phys*., 1984, **81**, 5577.
17 R. C. Macdonald and K. Liu, *J. Chem. Phys*., 1989, **91**, 821.
18 D. M. Sonnenfroh, R. G. Macdonald and K. Liu, *J. Chem. Phys*., 1991, **94**, 6508.
19 V. I. Veksler, *J. Phys. (USSR)*, 1945, **9**, 153.
20 E. M. McMillan, *Phys. Rev*., 1945, **68**, 143.
21 H. L. Bethlem, G. Berden, A. J. A. van Roij, F. M. H. Crompvoets and G. Meijer, *Phys. Rev. Lett*., 2000, **84**, 5744.
22 D. Auerbach, E. E. A. Bromberg and L. Wharton, *J. Chem. Phys*., 1966, **45**, 2160.
23 S. Y. T. van de Meerakker, N. Vanhaecke, H. L. Bethlem and G. Meijer, *Phys. Rev. A*, 2006, **73**, 023401.
24 F. M. H. Crompvoets, R. T. Jongma, H. L. Bethlem, A. J. A. van Roij and G. Meijer, *Phys. Rev. Lett*., 2002, **89**, 093004.
25 H. L. Bethlem, F. M. H. Crompvoets, R. T. Jongma, S. Y. T. van de Meerakker and G. Meijer, *Phys. Rev. A*, 2002, **65**, 053416.
26 H. L. Bethlem and G. Meijer, *Int. Rev. Phys. Chem*., 2003, **22**, 73.
27 E. A. Cornell and C. E. Wiemann, *Rev. Mod. Phys*., 2002, **74**, 875.
28 W. Ketterle, *Rev. Mod. Phys*., 2002, **74**, 1131.
29 F. M. H. Crompvoets, H. L. Bethlem and G. Meijer, *Adv. At. Mol. Opt. Phys*., ed. P. R. Berman and C. C. Lin, ISBN 0-12-003852-8, 2005, 52, 209–287.
30 J. R. Bochinski, E. R. Hudson, H. J. Lewandowski, G. Meijer and J. Ye, *Phys. Rev. Lett*., 2003, **91**, 243001.
31 S. Y. T. van de Meerakker, P. H. M. Smeets, N. Vanhaecke, R. T. Jongma and G. Meijer, *Phys. Rev. Lett*., 2005, **94**, 023004.
32 E. R. Hudson, C. Ticknor, B. C. Sawyer, C. A. Taatjes, H. J. Lewandowski, J. R. Bochinski, J. L. Bohn and J. Ye, *arXiv: physics/0508120*, 2005.
33 S. Y. T. van de Meerakker, I. Labazan, S. Hoekstra, J. Küpper and G. Meijer, *arXiv: physics/0512194*, 2005.
34 S. Jung, E. Tiemann and C. Lisdat, submitted.
35 T. P. Softley, S. R. Procter, Y. Yamakita, G. Maguire and F. Merkt, *J. Electron Spectrosc. Relat. Phenom*., 2005, **144**, 113.
36 E. Vliegen, H. J. Wörner, T. P. Softley and F. Merkt, *Phys. Rev. Lett*., 2004, **92**, 033005.
37 M. R. Tarbutt, H. L. Bethlem, J. J. Hudson, V. L. Ryabov, V. A. Ryzhov, B. E. Sauer, G. Meijer and E. A. Hinds, *Phys. Rev. Lett*., 2004, **92**, 173002.
38 M. Tarbutt and E. Hinds, private communications.

